Biol Trace Elem Res (2014) 159:416–424
DOI 10.1007/s12011-014-9972-0

Iron Oxide Nanoparticles Induce Oxidative Stress, DNA Damage, and Caspase Activation in the Human Breast Cancer Cell Line

Saud Alarifi · Daoud Ali · Saad Alkahtani · M. S. Alhader

Received: 1 March 2014 / Accepted: 8 April 2014 / Published online: 22 April 2014

Abstract Broad applications of iron oxide nanoparticles require an improved understanding of their potential effects on human health. In the present study, we explored the underlying mechanism through which iron oxide nanoparticles induce toxicity in human breast cancer cells (MCF-7). MTT (3-(4, 5-dimethylthiazol-2-yl)-2, 5-diphenyltetrazolium bromide) and lactate dehydrogenase assays were used to examine mechanisms of cytotoxicity. Concentration- and time-dependent cytotoxicity was observed in MCF-7 cells. Iron oxide nanoparticles were found to induce oxidative stress evidenced by the elevation of reactive oxygen species generation, lipid peroxidation, and depletion of superoxide dismutase, glutathione, and catalase activities in MCF-7 cells. Nuclear staining was performed using 4′, 6-diamidino-2-phenylindole (DAPI), and cells were analyzed with a fluorescence microscope. Iron oxide nanoparticles (60 μg/ml) induced substantial apoptosis that was identified by morphology, condensation, and fragmentation of the nuclei of the MCF-7 cells. It was also observed that the iron oxide NPs induced caspase-3 activity. DNA strand breakage was detected by comet assay, and it occurred in a concentration- and time-dependent manner. Thus, the data indicate that iron oxide nanoparticles induced cytotoxicity and genotoxicity in MCF-7 cells via oxidative stress. This study warrants more careful assessment of iron oxide nanoparticles before their industrial applications.

Keywords Iron oxide nanoparticles · MCF-7 cells · Oxidative stress · Apoptosis · DNA damage

Introduction

The use of magnetic nanoparticles in clinical medicine is an important field in the various areas of therapeutics. The iron oxide nanoparticles are of high interest for in vivo applications, including magnetic resonance imaging for medical diagnosis, hyperthermia in cancer therapy, tissue repair, drug delivery, and cellular therapy. In Saudi Arabia, breast cancer is the second leading cause of cancer death in women and the risk of its incidence is increasing every year [1]. Jain [2] reported that iron oxide nanoparticles increased alanine aminotransferase, aspartate aminotransferase, and alkaline phosphatase levels in rats. Due to the wide use of iron oxide nanoparticles in manufacturing industries, concerns about their potential toxic effects in humans and the environment have increased. However, the molecular mechanisms by which iron oxide nanoparticles induce cytotoxicity remain unexplored.

In anticancer studies, magnetic nanoparticles are widely used in medical examinations, targeting, and treatment [3]. Magnetic nanoparticles are considered good carriers of many chemotherapeutic agents [4]. In vivo injection of doxorubicin-loaded magnetic nanoparticles intramurally into mice implanted subcutaneously with lung carcinoma has resulted in an increase in the efficacy of doxorubicin against tumors [5]. Due to their small size and surface properties, nanoparticles may cross biological barriers to reach different tissues; hence, accumulation of metal nanoparticles was previously observed in many different organs [6]. Their potential toxicological

Daoud Ali and Saud Alarifi contributed equally to this work.

S. Alarifi · D. Ali (✉) · S. Alkahtani
Department of Zoology, College of Science, King Saud University, Box 2455, Riyadh 11451, Saudi Arabia
e-mail: daudali.ksu12@yahoo.com

D. Ali
e-mail: aalidaoud@ksu.edu.sa

M. S. Alhader
King Abdul-Aziz City for Science and Technology, Riyadh, Saudi Arabia

impacts are still a matter of investigation, and our actual knowledge on the effects of nano-sized particles on biological systems remains incomplete [7, 8].

Recent studies reported on nanoparticle-induced oxidative stress as determined by increasing membrane lipid peroxidation (LPO) and reactive oxygen species (ROS) and decreasing intracellular glutathione (GSH) [9]. Oxidative stress plays an important role in cellular signaling and inflammatory, genotoxic, and proliferative responses [10, 11]. Superoxide dismutase, catalase, and GSH reductase are known natural antioxidants that neutralize excessive ROS and prevent it from damaging the cellular structure [12]. We evaluated these oxidative stress biomarkers including reduced GSH, superoxide dismutase, and catalase; ROS generation; and malondialdehyde as an end product of membrane lipid peroxidation in response to iron oxide nanoparticle exposure.

Therefore, the current study was designed to assess the cellular toxicity and genotoxic potential of iron oxide nanoparticles in human breast cancer cells as well as to understand their possible mechanisms.

Materials and Methods

Chemicals and Reagents

Iron oxide (Fe_2O_3) nanoparticles (Product No. 544884 and APS <50 nm), GSH, 5, 5-dithio-bis-(2-nitrobenzoic acid) (DTNB), 3-(4, 5-dimethylthiazol-2-yl)-2, 5-diphenyltetrazolium bromide (MTT), 2, 7-dichlorofluorescin diacetate (DCFH-DA), propidium iodide, and 4′, 6-diamidino-2-phenylindole (DAPI) were obtained from Sigma-Aldrich. Fetal bovine serum, penicillin-streptomycin, and Dulbecco's modified Eagle medium (DMEM)/F-12 were purchased from Invitrogen (Carlsbad, CA, USA). All other chemicals used were of the highest purity and available from commercial sources.

Iron Oxide Nanoparticle Preparation and Characterization

Iron oxide nanoparticles were suspended in Milli-Q water (EMD Millipore, Billerica, MA, USA) at a concentration of 1 mg/ml. Stock suspension was sonicated at 40 W for 15 min. Samples for transmission electron microscopy (TEM) analysis were prepared by drop-coating the iron oxide nanoparticle suspension on carbon-coated copper TEM grids. The films on the TEM grids were allowed to dry prior to measurement. TEM measurements were performed on a JEOL model 2100 F (JEOL, Tokyo, Japan) instrument operated at an accelerating voltage of 200 kV.

Cell Culture and Exposure of Iron Oxide Nanoparticles

Human breast cancer cells (MCF-7) were procured from the American Type Culture Collection, Rockville, MD, USA, and they were preserved and subcultured in the laboratory and used to determine cytotoxicity against iron oxide nanoparticles. Cells were cultured in the DMEM/F-12 medium supplemented with 10 % FBS and 100 U/ml penicillin-streptomycin at 5 % CO_2 and 37 °C. At 85 % confluence, cells were harvested by using 0.25 % trypsin and were subcultured into 75-cm^2 flasks, six-well plates, and 96-well plates according to experiments. Cells were allowed to attach to the surface for 24 h prior to treatment. Iron oxide nanoparticles were suspended in the cell culture medium and diluted to appropriate concentrations (0, 10, 30, 60, and 120 μg/ml). The appropriate dilutions of iron oxide nanoparticles were sonicated using a sonicator bath at room temperature for 10 min at 40 W to avoid particle agglomeration before exposure to the cells. Cells not exposed to iron oxide nanoparticles served as control in each experiment.

Cell Morphology

The morphology of MCF-7 cells was observed after the exposure of iron oxide nanoparticles for 24 and 48 h by using a Leica DM IL phase-contrast microscope (Leica Microsystems, Wetzlar, Germany).

MTT Assay

MTT assay was used to investigate mitochondrial function as described by Mossman [13]. Briefly, 1×10^4 cells/well were seeded in 96-well plates and exposed to different concentrations (0, 10, 30, 60, and 120 μg/ml) of iron oxide nanoparticles for 24 and 48 h. At the end of the exposure, culture media were replaced with new media containing MTT solution (0.5 mg/ml) and incubated for 4 h at 37 °C. As a result, formazan crystal was formed, and it was dissolved in DMSO. The plates were kept on a shaker for 10 min at room temperature and then analyzed at 530 nm using a multiwell microplate reader (Omega Fluostar, BMG Labtech GmbH, Allmendgruen, Germany). Untreated sets were also run under identical conditions and served as controls.

Lactate Dehydrogenase Leakage Assay

The release of cytoplasmic lactate dehydrogenase enzyme (LDH) into the culture medium was determined by Wroblewski and LaDue [14]. MCF-7 cells were treated with different concentrations (0, 10, 30, 60, and 120 μg/ml) of iron oxide nanoparticles for 24 and 48 h. After exposure, 100-μl samples from the centrifuged culture media were collected. The LDH activity was assayed in 3.0 ml of reaction mixture

with 100 μl of pyruvic acid (2.5 mg/ml phosphate buffer) and 100 μl of NADH (2.5 mg/ml phosphate buffer) and the rest of the volume adjusted with phosphate buffer (0.1 M, pH 7.4). The rate of NADH oxidation was determined by following the decrease in absorbance at 340 nm for 3 min at 1-min intervals at 25 °C using a spectrophotometer (Varian, Cary 300 Bio). The amount of LDH released is expressed as LDH activity (IU/l) in culture media.

Measurement of Intracellular ROS

ROS generation was assessed in MCF-7 cells after exposure to different concentrations (0, 10, 30, 60, and 120 μg/ml) of iron oxide nanoparticles by using DCFH-DA dye as fluorescence agent [15]. The cells (1×10^4 per well) were seeded in 96-well black bottom culture plates and allowed to adhere to them for 24 h in a CO_2 incubator at 37 °C. Then, MCF-7 cells were exposed to the above concentrations of iron oxide nanoparticles for 24 and 48 h. After exposure, cells were incubated with DCFH-DA (10 mM) for 30 min at 37 °C. The reaction mixture was aspirated and replaced by 200 μl of phosphate-buffered saline (PBS) in each well. The plates were kept on a shaker for 10 min at room temperature in the dark. Fluorescence intensity was measured using a multiwell microplate reader (Omega Fluostar) at excitation wavelength 485 nm and at emission wavelength 528 nm, and values were expressed as percent of fluorescence intensity relative to control wells.

A parallel set of cells (5×10^4 per well) was analyzed for intracellular fluorescence using an upright fluorescence microscope equipped with a CCD cool camera (Nikon Eclipse 80i with Nikon DS-Ri1 12.7 megapixel camera; Nikon Corporation, Tokyo, Japan).

Oxidative Stress Biomarkers

Cells at a final density of ~6×10^6 in a 75-cm^2 culture flask were exposed to 0, 10, 30, 60, and 120 μg/ml of iron oxide nanoparticles for 24 and 48 h. After exposure, the cells were scraped and washed twice with chilled 1× PBS. The harvested cell pellets were lysed in cell lysis buffer [20 mM Tris–HCl (pH 7.5), 150 mM NaCl, 1 mM Na_2EDTA, 1 % Triton, and 2.5 mM sodium pyrophosphate]. The cells were centrifuged at 15,000*g* for 10 min at 4 °C, and the supernatant (cell extract) was maintained on ice until assayed for oxidative stress biomarkers. Protein content was measured by the method of Bradford [16] using bovine serum albumin as the standard.

LPO Assay

The extent of membrane lipid peroxidation was estimated by measuring the formation of malondialdehyde (MDA) using the method of Ohkawa et al. [17]. A mixture of 0.1 ml cell extract and 1.9 ml of 0.1 M sodium phosphate buffer (pH 7.4) was incubated at 37 °C for 1 h. The incubation mixture, after precipitation with 5 % TCA, was centrifuged (2,300*g* for 15 min at room temperature) and the supernatant collected. Then, 1.0 ml of 1 % TBA was added to the supernatant and placed in boiling water for 15 min. After cooling to room temperature, absorbance of the mixture was taken at 532 nm and expressed in MDA (nmol/mg protein) using a molar extinction coefficient of 1.56×10^5 M/cm.

Glutathione Estimation

The GSH level was quantified by using Ellman's reagent [18]. The assay mixture contained phosphate buffer, DTNB, and cell extract. The reaction was monitored at 412 nm, and the amount of GSH was expressed in terms of nanomoles of GSH per milligram of protein.

Measurement of Superoxide Dismutase

The assay mixture contained sodium pyrophosphate buffer, nitro blue tetrazolium (NBT), phenazine methosulfate, reduced nicotinamide adenine dinucleotide, and the required volume of cell extract, and the absorbance of the reaction mixture was measured at 450 nm.

Measurement of Catalase Activity

Catalase activity was measured by its ability to split hydrogen peroxide (H_2O_2) within 1 min of incubation time. The reaction was stopped by adding dichromate/acetic acid reagent, and the remaining H_2O_2 was determined by measuring chromic acetate at 570 nm which is formed by the reduction of dichromate/acetic acid in the presence of H_2O_2 as described earlier by Sinha [19]. Catalase activity was expressed as micromoles of H_2O_2 decomposed per minute per milligram of protein.

DAPI Staining for Chromosome Condensation

Chromosome condensation in MCF-7 cells due to iron oxide nanoparticle exposure was observed by DAPI staining according to the method described by Alarifi et al. [20]. DAPI solution was used to stain the exposed cells in eight chamber slides, and the slides were incubated for 10 min in the dark at 37 °C. Images of the nucleus were captured using a fluorescence microscope (Nikon Eclipse 80i with Nikon DS-Ri1 12.7 megapixel camera; Nikon Corporation, Tokyo, Japan).

Caspase-3 Assay

The activity of caspase-3 was determined from the cleavage of the caspase-3 substrate (*N*-acetyl-DEVD-*p*-nitroaniline). The *p*-nitroaniline was used as the standard. Cleavage of the

substrate was monitored at 405 nm, and the specific activity was expressed in picomoles of the product (nitroaniline) per minute per milligram of protein.

Determination of DNA Damage

The alkaline single-cell gel electrophoresis (SCGE) was performed as a three-layer procedure [21]. In brief, 70,000 cells/well were seeded in a six-well plate. After 24 h of seeding, cells were treated with different concentrations of iron oxide nanoparticles for 24 and 48 h. After treatment, the MCF-7 cells were trypsinized and suspended in DMEM, and the cell suspension was centrifuged at 1,200 rpm at 4 °C for 5 min. The cell pellet was finally suspended in chilled phosphate buffer saline for comet assay. The samples showing cell viability higher than 84 % were further processed for comet assay. In brief, about 15 μl of cell suspension (approx. 20,000 cells) was mixed with 85 μl of 0.5 % low-melting-point agarose and layered on one end of a frosted plain glass slide, precoated with a layer of 200 μl normal agarose (1 %). Thereafter, it was covered with a third layer of 100 μl low-melting-point agarose. After solidification of the gel, the slides were immersed in lysing solution (2.5 M NaCl, 100 mM Na_2EDTA, 10 mM Tris pH 10 with 10 % DMSO and 1 % Triton X-100 added fresh) overnight at 4 °C. The slides were then placed in a horizontal gel electrophoresis unit. Fresh cold alkaline electrophoresis buffer (300 mM NaOH, 1 mM Na_2EDTA, and 0.2 % DMSO, pH 13.5) was poured into the chamber and left for 20 min at 4 °C for DNA unwinding and conversion of alkali-labile sites to single-strand breaks. Electrophoresis was carried out using the same solution at 4 °C for 20 min, at 15 V (0.8 V/cm) and 300 mA. The slides were neutralized gently with 0.4 M Tris buffer at pH 7.5 and stained with 75 μl ethidium bromide (20 μg/ml). For positive control, the MCF-7 cells were treated with 100 μM H_2O_2 for 10 min at 4 °C. Two slides were prepared from each well (per concentration), and 50 cells per slide (100 cells per concentration) were scored randomly and analyzed using an image analysis system (Komet 5.0, Kinetic Imaging, Liverpool, UK) attached to a fluorescence microscope (DMLB, Leica, Germany) equipped with appropriate filters. The parameters, e.g., percent tail DNA (% tail DNA = 100 − % head DNA) and olive tail moment, were selected for quantification of DNA damage in MCF-7 cells as determined by the software (Komet 5.0; Kinetic Imaging, Liverpool, UK).

Statistical Analysis

At least three independent experiments were carried out for each evaluation. Data were expressed as mean (±SE) and analyzed by one-way analysis of variance (ANOVA). A p value less than 0.05 was considered statistically significant.

Results

Iron Oxide Nanoparticles

Figure 1a showed a typical TEM image of the iron oxide nanoparticles. From the image, it can be seen that the majority of the particles were spherical in shape with smooth surfaces.

Morphological Changes

Figure 2 showed the comparative morphology of untreated and iron oxide nanoparticle-treated MCF-7 cells. Cells treated with 30 μg/ml iron oxide nanoparticles changed into spherical shape and detached from the surface (Fig. 2b).

Iron Oxide Nanoparticles Induced Cytotoxicity in MCF-7 Cells

We examined mitochondrial function (MTT reduction) and membrane damage (LDH leakage) as cytotoxicity end points. MTT results demonstrated concentration- and time-dependent cytotoxicity after exposure to iron oxide nanoparticles in MCF-7 cells (Fig. 3a). The percentage of cell viability (relative to control) observed after 24 h of exposure at concentrations 10, 30, 60, and 120 μg/ml of iron oxide nanoparticles was 99, 84, 67.4, and 46.9 % with a further reduction to 98.6, 70, 57.8, and 39 % after 48 h of exposure, respectively.

Lactate dehydrogenase enzyme release, a marker of cell membrane damage, was measured in MCF-7 cells exposed to iron oxide nanoparticles at concentrations of

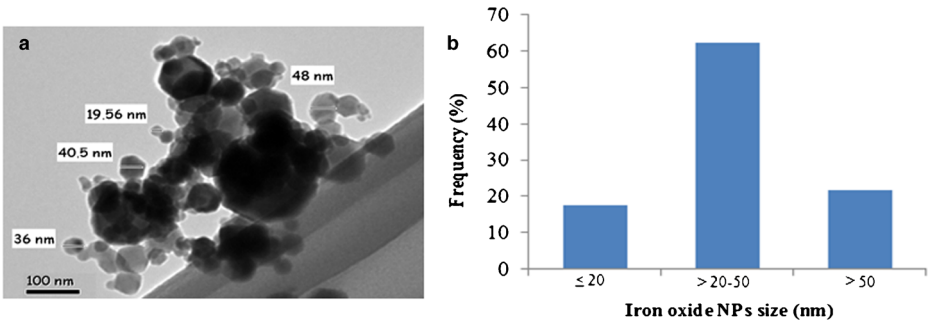

Fig. 1 Characterization of iron oxide nanoparticles. **a** TEM image. **b** A size distribution histogram generated by using the TEM image

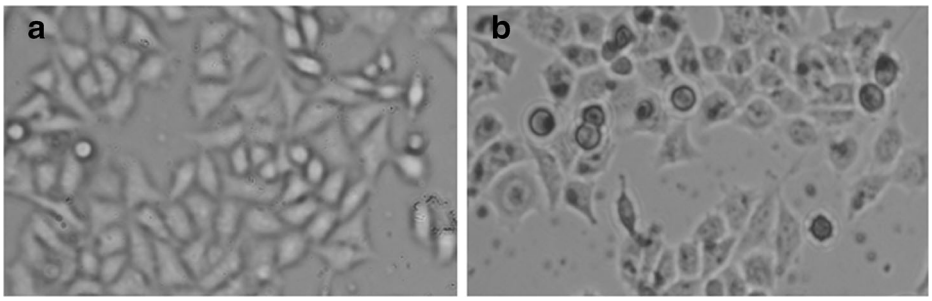

Fig. 2 Morphology of human breast cancer cells (MCF-7). **a** Control. **b** Treatment with 30 μg/ml of iron oxide nanoparticles

0, 10, 30, 60, and 120 μg/ml for 24 and 48 h. However, as the concentration of iron oxide nanoparticles increased, significant LDH leakage was observed in a dose- and time-dependent manner (Fig. 3b).

Iron Oxide Nanoparticles Induced ROS Generation and Oxidative Stress

The ability of iron oxide nanoparticles to induce oxidative stress was evaluated by measuring the levels of ROS, LPO, GSH, superoxide dismutase, and catalase in MCF-7 cells. Results showed that iron oxide nanoparticles induced intracellular ROS generation in a dose- and time-dependent manner (Fig. 4). Iron oxide nanoparticle-induced oxidative stress was further evidenced by depletion of GSH, superoxide dismutase, and catalase (Fig. 5b–d) and elevation of LPO with increased concentrations of and time of exposure to iron oxide nanoparticles (Fig. 5a).

Induction of Chromosomal Condensation and Caspase-3 Activity by Iron Oxide Nanoparticles

Chromatin condensation was determined by DAPI staining. MCF-7 cells treated with iron oxide nanoparticles at the abovementioned concentrations for 24 h produced chromatin condensation (Fig. 6a, b).

Caspase-3, which plays a key role in the apoptotic pathway of cells, was induced following treatment with iron oxide nanoparticles (Fig. 6c). When cells were treated with 10, 30, and 60 μg/ml concentrations of iron oxide nanoparticles for 24 and 48 h, the activity of caspase-3 was increased in a concentration- and time-dependent manner.

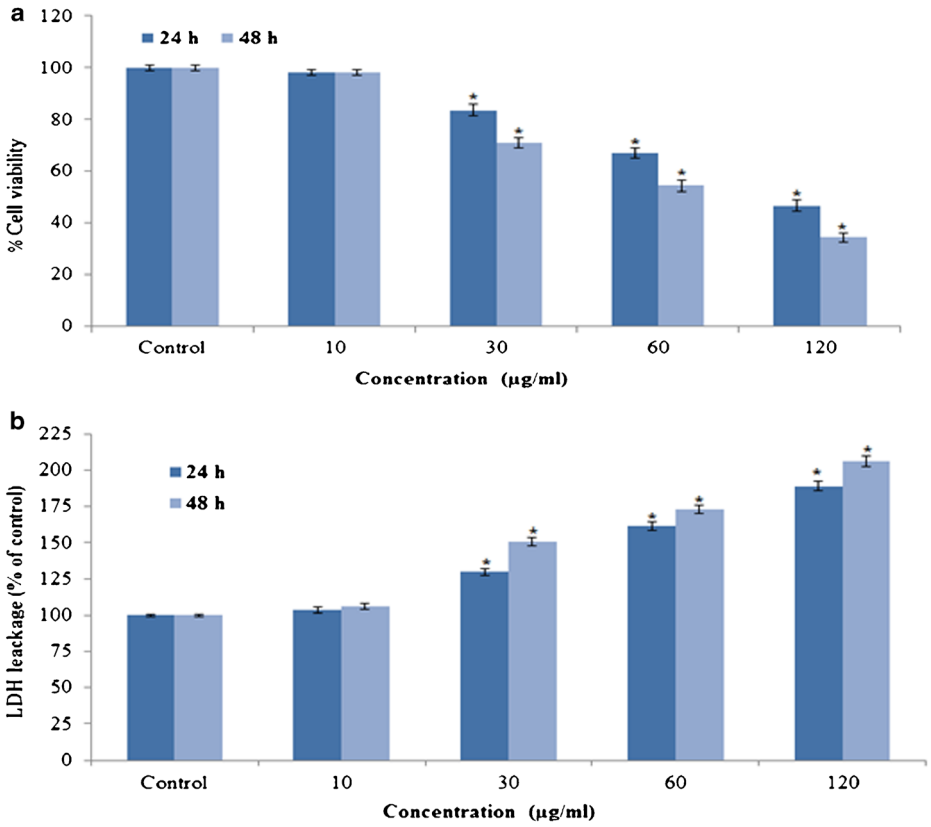

Fig. 3 Cytotoxicity of iron oxide nanoparticles on MCF-7 cells. **a** Percent cell viability. **b** LDH leakage. Each value represents the mean ± SE of three experiments.*$p<0.05$ vs. control

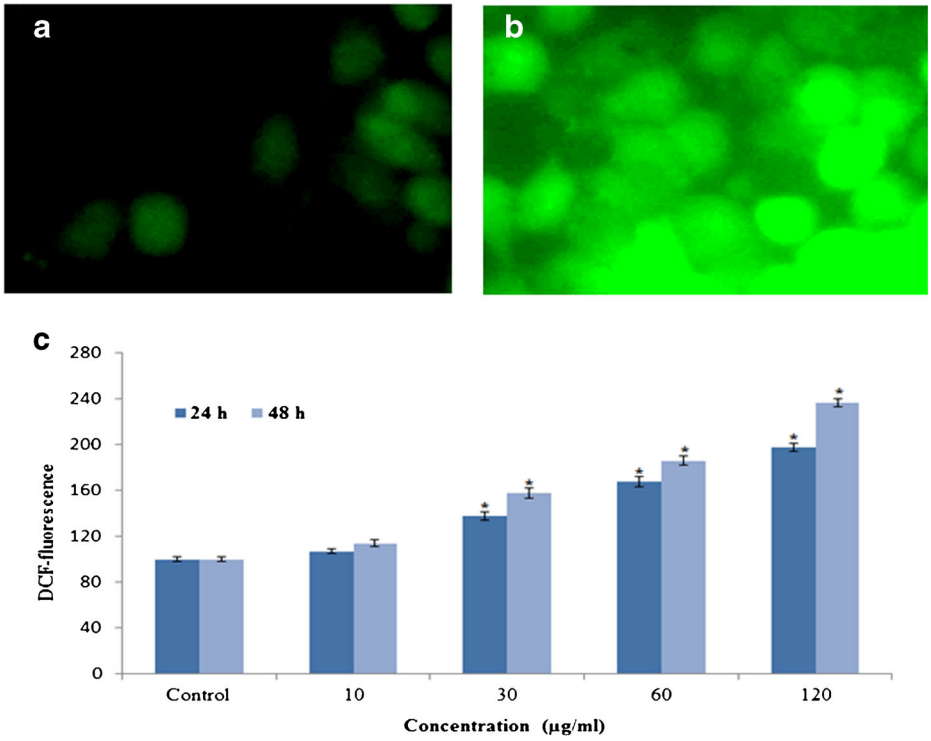

Fig. 4 Iron oxide nanoparticles induced ROS generation in MCF-7 cells. **a** Percentage of ROS generation at different concentrations of iron oxide nanoparticles in MCF-7 cells. **b** Control. **c** At 120 µg/ml of iron oxide nanoparticles. *Images* were snapped in a Nikon phase-contrast cum fluorescence microscope (model 80i). Each value represents the mean ± SE of three experiments.*$p<0.05$ vs. control

DNA Damage

DNA damage was measured as percent tail DNA and olive tail moment in the control as well as exposed cells. The cells exposed to different doses of iron oxide nanoparticles exhibited significantly ($p>0.05$) higher DNA damage than those of the control groups. The gradual nonlinear increase in DNA damage was observed in cells as dose and time of iron oxide nanoparticle exposure increased. The highest DNA damage was recorded at 60 µg/ml iron oxide nanoparticles in MCF-7 cells (Fig. 7).

Discussion

Iron oxide nanoparticles have been used comprehensively in industrial fields, and concerns about their potential toxicity to humans and their environmental impact have increased rapidly. Our results demonstrate that iron oxide nanoparticles have cytotoxic and genotoxic effects on MCF-7 cells. The results also revealed that the mode of cell death was apoptosis which was mediated by the ROS-triggered mitochondrial pathway as evidenced by cleavage of caspase-3 activity. Before studying the cytotoxicity and genotoxic potential of the iron oxide

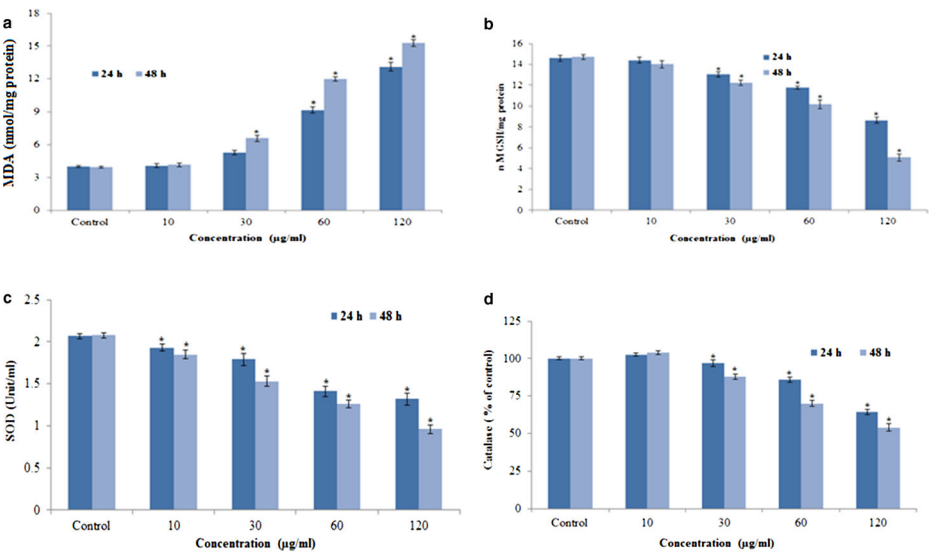

Fig. 5 **a** Levels of lipid peroxides. **b** GSH. **c** Superoxide dismutase. **d** Catalase in MCF-7 cells after exposure to iron oxide nanoparticles. Each value represents the mean±SE of three experiments.*$p<0.05$ vs. control

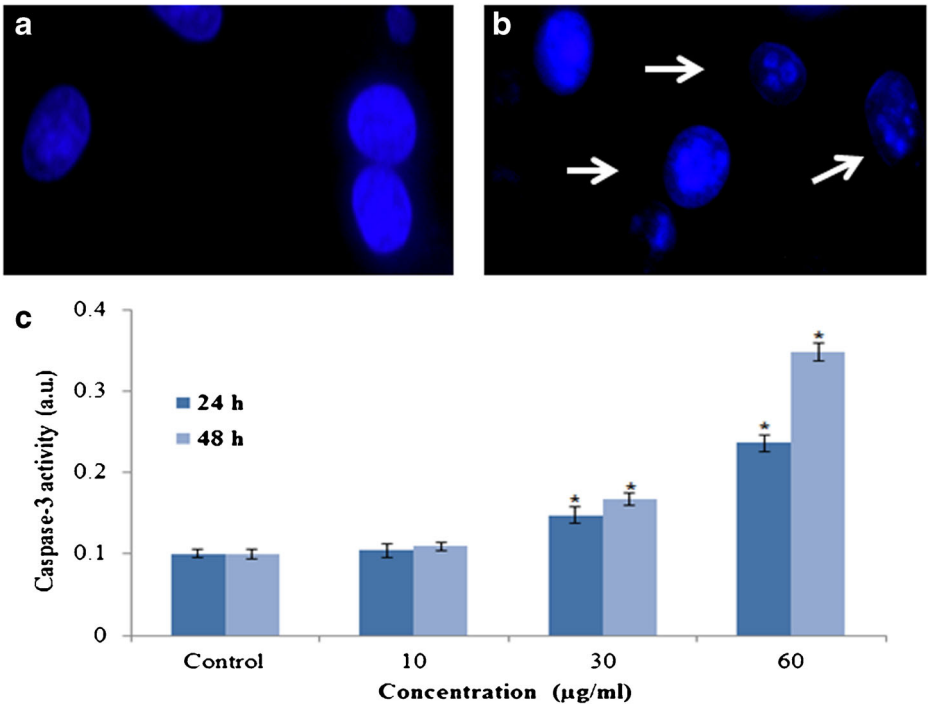

Fig. 6 Induction of chromosomal condensation and caspase-3 activity in MCF-7 cells after exposure to iron oxide nanoparticles for 24 and 48 h. **a** Control (viable) cell. **b** Exposed at 60 µg/ml of iron oxide nanoparticles. **c** Caspase-3 activity. Each value represents the mean±SE of three experiments. *$p<0.05$ vs. control

nanoparticles, we characterized their size through TEM. The interference of some nanoparticles with commonly used cytotoxicity test systems has been well reported in the literature. Therefore, it has been suggested that the cytotoxicity of nanoparticles should be assessed with two or more independent test systems for validating the findings [22]. We have evaluated the cytotoxicity of iron oxide nanoparticles using two different assays, e.g., MTT and LDH release, to increase the strength of the data. In the present study, iron oxide nanoparticles induced cytotoxicity in a dose- and time-dependent manner.

It has been reported that nanoparticles of various sizes and different chemical compositions attack mitochondria, which are redox-active organelles [23]. Mitochondria are a prominent site of ROS formation in cells exposed to nanoparticles [24]. Therefore, nanoparticles may change the production of ROS and affect antioxidant defenses to induce oxidative stress [25]. To determine if iron oxide nanoparticles induce oxidative stress in MCF-7 cells, we measured ROS, the level of MDA, and superoxide dismutase, GSH, and catalase activities. The generation of ROS and MDA were found to be increased significantly. On the other hand, superoxide dismutase, GSH, and catalase activities were reduced. The increased levels of ROS have been found to negatively disrupt the balance between oxidation and antioxidant defense systems, which leads to apoptosis via oxidative damage to intracellular proteins and DNA and increased LPO [26]. Thus, damage could accumulate more rapidly in mitochondria than in the rest of the cellular components [27]. To counteract these adverse effects, cells utilize antioxidant enzymes such as superoxide dismutase, GSH, and catalase to remove the

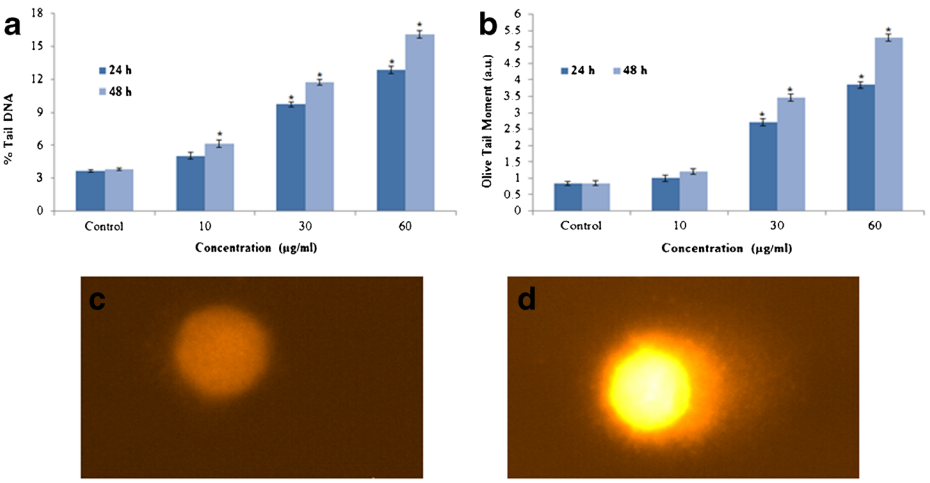

Fig. 7 DNA damage in MCF-7 cells at different concentrations of iron oxide nanoparticles. **a** Percent tail DNA. **b** Olive tail moment. **c** Control cell. **d** Exposed cell. Each value represents the mean ± SE of three experiments. *$p<0.05$ vs. control

redundant ROS. In the present study, the increased production of ROS and MDA and the reduced activity of the antioxidant enzymes superoxide dismutase, GSH, and catalase suggested that iron oxide nanoparticles caused imbalances between the production and degradation of ROS and induced oxidative stress, changes which may result in cell damage and apoptosis. Free oxygen radical generation and oxidative stress elicit a wide variety of cellular events including DNA damage and apoptosis [28]. This has been attributed to their small size and large surface area which is generally thought to produce ROS and oxidative stress [29]. ROS typically include the superoxide radical (O^{2-}), hydrogen peroxide (H_2O_2), and the hydroxyl radical ($OH^{\cdot}$) which cause damage to cellular components including DNA damage and ultimately apoptotic cell death [30]. This observation is consistent with earlier studies by Alarifi et al. [31] which have shown similar effects of nickel nanoparticles on human skin epidermal cells. LPO can further give rise to more free radicals and damage biomolecules like DNA, proteins, and lipids in conjunction with ROS. Nel et al. [32] had reported that LPO and oxidative stress is one of the more important mechanisms of toxicity related to nanoparticles. Iron oxide nanoparticles cause injury to the cell membrane as indicated by an increased level of lactate dehydrogenase enzyme release. Our results are consistent with the findings of other investigators demonstrating that metal oxide nanoparticles have the potential to induce DNA damage [33].

Iron oxide nanoparticle-induced cell death observed in this study can occur by apoptosis which can be distinguished by morphological and biochemical features. Iron oxide nanoparticles in our study also activated caspase-3, and the activity was increased to about 230 % of the level of the control group when the cells were treated with 60 μg/ml for 48 h. The activation of caspase-3 was seen in a dose- and time-dependent manner from 10 to 60 μg/ml. The activation signal of caspase-3 seemed to be through the induction of ROS, which is the general pathway of toxic chemicals to induce ROS generation. Many other chemicals, which have cytotoxicity through the apoptotic mechanism, showed increased ROS and caspase-3 activity. Cadmium and mercury also show ROS induction and caspase-3 activity and then, finally, apoptosis in cultured cells [34]. DAPI staining of iron oxide nanoparticle-treated MCF-7 cells resulted in nuclear condensation and fragmentation which is another morphological hallmark of apoptosis. Porter [35] had reported that caspase-3 activation may cause chromosome condensation and also DNA fragmentation to trigger apoptosis of cells. Chen and Mikecz [36] reported that nanoparticles due to their small size are capable of reaching the nucleus and interacting with DNA. They may also exhibit an indirect effect on DNA through their ability to generate ROS. This DNA damage may either induce carcinogenesis or cell death, thus disrupting normal cell functions. We detected the genotoxic potential of iron oxide nanoparticles in MCF-7 cells by comet assay which is capable of detecting single as well as double DNA strand breaks and alkali-labile sites even at low levels of DNA damage [37]. Martinez et al. [38] have reported that ROS are involved in DNA damage causing damage to both purine and pyrimidine bases as well as the DNA backbone.

Our results demonstrate that iron oxide nanoparticles induce cell death and DNA damage in human breast cancer cells, which may be mediated through the ROS and oxidative stress.

Acknowledgments The authors would like to extend their sincere appreciation to the Deanship of Scientific Research at King Saud University for funding this research through research group Project No. RGP-VPP-180.

Conflict of Interest None.

References

1. Alghamdi IG, Hussain II, Alghamdi MS, El-Sheemy MA (2013) The incidence rate of female breast cancer in Saudi Arabia: an observational descriptive epidemiological analysis of data from Saudi Cancer Registry 2001-2008. Breast Cancer Targets Ther 5:103–109
2. Jain TK, Reddy MK, Morales MA, Leslie-Pelecky DL, Labhasetwar V (2008) Biodistribution, clearance, and biocompatibility of iron oxide magnetic nanoparticles in rats. Mol Pharm 5(2):316–327
3. Lee KJ, An JH, Shin JS, Kim DH (2012) Synthesis and characterization of bicalutamide-loaded magnetic nanoparticles as anti-tumor drug carriers. J Nanosci Nanotechnol 12(2):1611–1615
4. Maeng JH, Lee DH, Jung KH, Bae YH, Park IS, Jeong S, Jeon YS, Shim CK, Kim W, Kim J, Lee J, Lee YM, Kim JH, Kim WH, Hong SS (2010) Multi-functional doxorubicin-loaded super paramagnetic iron oxide nanoparticles for chemotherapy and magnetic resonance imaging in liver cancer. Biomaterials 31(18):4995–5006
5. Jia Y, Yuan M, Yuan H, Huang X, Sui X, Cui X, Tang F, Peng J, Chen J, Lu S, Xu W, Zhang L, Guo Q (2012) Co-encapsulation of magnetic Fe3O4 nanoparticles and doxorubicin into biodegradable PLGA nanocarriers for intratumoral drug delivery. Int J Nanomedicine 63: 1697–1708
6. Li Y-F, Chen C (2011) Fate and toxicity of metallic and metal-containing nanoparticles for biomedical applications. Small 7: 2965–2980
7. Singh N, Manshian B, Jenkins GJS, Griffiths SM, Williams PM, Maffeis TG, Wright CJ, Doak SH (2009) Nano genotoxicology: the DNA damaging potential of engineered nanomaterials. Biomaterials 30:3891–3914
8. Skocaj M, Filipic M, Petkovic J, Novak S (2011) Titanium dioxide in our everyday life; is it safe? Radiol Oncol 45:227–247
9. Wang Y, Aker WG, Hwang HM, Yedjou CGYH et al (2011) A study of the mechanism of in vitro cytotoxicity of metal oxide nanoparticles using catfish primary hepatocytes and human HepG2 cells. Sci Total Environ 409:4753–4762
10. van Maanen JM, Borm PJ, Knaapen A, van Herwijnen M, Schilderman PA, Smith KR, Aust AE, Tomatis M, Fubini B (1999) In vitro effects of coal fly ashes: hydroxyl radical generation, iron release, and DNA damage and toxicity in rat lung epithelial cells. Inhal Toxicol 11:1123–1141
11. Borm PJ, Schins RP, Albrecht C (2004) Inhaled particles and lung cancer, part B: paradigms and risk assessment. Int J Cancer 110:3–14

12. Naziroglu M, Simsek M, Kutlu M (2004) Moderate exercise with dietary vitamin C and E combination protects streptozotocin induced oxidative damage to the blood and improves fetal outcomes in pregnant rats. Clin Chem Lab Med 42:511–517
13. Mossman T (1983) Rapid colorimetric assay for cellular growth and survival: application to proliferation and cytotoxicity assays. J Immunol Methods 65:55–63
14. Wroblewski F, LaDue JS (1955) Lactate dehydrogenase activity in blood. Proc Soc Exp Biol Med 90:210–213
15. Wang H, Joseph JA (1999) Quantifying cellular oxidative stress by dichlorofluorescein assay using microplate reader. Free Radic Biol Med 27:612–616
16. Bradford MM (1976) A rapid and sensitive method for the quantitation of microgram quantities of protein utilizing the principle of protein-dye binding. Anal Biochem 72:248–254
17. Ohkawa H, Ohishi N, Yagi K (1979) Assay for lipid peroxides in animal tissues by thiobarbituric acid reaction. Anal Biochem 95:351–358
18. Ellman G (1959) Tissue sulfhydryl groups. Arch Biochem Biophys 82:70–77
19. Sinha AK (1972) Colorimetric assay of catalase. Anal Biochem 47: 389–394
20. Alarifi S, Ali D, Verma A, Alakhtani S, Ali BA (2013) Cytotoxicity and genotoxicity of copper oxide nanoparticles in human skin keratinocytes cells. Int J Toxicol 32(4):296–307
21. Ali D, Ray RS, Hans RK (2010) UVA-induced cyototoxicity and DNA damaging potential of benz (e) acephenanthrylene in human skin cell line. Toxicol Lett 199(2):193–200
22. Monteiro-Riviere NA, Inman AO, Zhang LW (2009) Limitations and relative utility of screening assays to assess engineered nanoparticle toxicity in a human cell line. Toxicol Appl Pharmacol 234(2):222–235
23. Xia T, Kovochich M, Liong M, Mädler L, Gilbert B, Shi H, Yeh JI, Zink JI, Nel AE (2008) Comparison of the mechanism of toxicity of zinc oxide and cerium oxide nanoparticles based on dissolution and oxidative stress properties. ACS Nano 2(10):2121–2134
24. Asha Rani PV, Mun GLK, Hande MP, Valiyaveettil S (2009) Cytotoxicity and genotoxicity of silver nanoparticles in human cells. ACS Nano 3(2):279–290
25. Srinivas A, Rao PJ, Selvam G, Murthy PB, Reddy PN (2011) Acute inhalation toxicity of cerium oxide nanoparticles in rats. Toxicol Lett 205:105–115
26. Naziroglu M, Uguz AC, Kocak A, Bal R (2009) Acetaminophen at different doses protects brain microsomal Ca^{2+}-ATPase and the antioxidant redox system in rats. J. Membr Biol 231:57–64
27. Brooks C, Wei Q, Feng L, Dong G, Tao Y, Mei L, Xie ZJ, Dong Z (2007) Bak regulates mitochondrial morphology and pathology during apoptosis by interacting with mitofusins. Proc Nat Acad Sci USA 104:11649–11654
28. Ostrovsky S, Kazimirsky G, Gedanken A, Brodie C (2009) Selective cytotoxic effect of ZnO nanoparticles on glioma cells. Nano Res 2: 882–890
29. Xia T, Kovochich M, Brant J, Hotze M, Sempf J, Oberley T et al (2006) Comparison of the abilities of ambient and manufactured nanoparticles to induce cellular toxicity according to an oxidative stress paradigm. Nano Lett 6(8):1794–1807
30. Ott M, Gogvadze V, Orrenius S, Zhivotovsky B (2007) Mitochondria, oxidative stress and cell death. Apoptosis 12:913–922
31. Alarifi S, Ali D, Alakhtani S, Al-Suhaibani ES, Al-Qahtani AA (2014) Reactive oxygen species-mediated DNA damage and apoptosis in human skin epidermal cells after exposure to nickel nanoparticles. Biol Trace Elem Res 157:84–93
32. Nel A, Xia T, Madler L, Li N (2006) Toxic potential of materials at the nano level. Science 311:622–627
33. Eom HJ, Choi J (2009) Oxidative stress of CeO2 nanoparticles via p38-Nrf-2 signaling pathway in human bronchial epithelial cell, BEAS-2B. Toxicol Lett 187:77–83
34. Park EJ, Park K (2007) Induction of reactive oxygen species and apoptosis in BEAS-2B cells by mercuric chloride. Toxicol in Vitro 21:789–794
35. Porter AG, Janicke RU (1999) Emerging roles of caspase-3 in apoptosis. Cell Death Differ 6:99–104
36. Chen M, Mikecz A (2005) Formation of nucleoplasmic protein aggregates impairs nuclear function in response to SiO_2 nanoparticles. Exp Cell Res 305(1):51–62
37. Collins AR (2004) The comet assay for DNA damage and repair: principles, applications and limitations. Mol Biotechnol 26(3):249–261
38. Martinez GR, Loureiro AP, Marques SA, Miyamoto S, Yamaguchi LF, Onuki J, Almeida EA, Garcia CC, Barbosa LF, Medeiros MH, Di Mascio P (2003) Oxidative and alkylating damage in DNA. Mutat Res 544:115–127